RESILIENT INFRASTRUCTURE
June 1–4, 2016
RESILIENT INFRASTRUCTURE LONDON 2016

FFECTS OF FINITE ELEMENT MODELLING APPROACH FOR PRESTRESSING SYSTEM ON THE PRESSURE CAPACITY OF A CANDU CONTAINMENT STRUCTURE

I. Tavakkoli
PhD Candidate, Ryerson University, Canada

M.R. Kianoush
Professor, Ryerson University, Canada

H. Abrishami
Lead Containment Structure Design, SNC-Lavalin, Inc., Canada

X. Han
Director, SNC-Lavalin, Inc., Canada

ABSTRACT

The primary objective of this article is to investigate the response of a CANDU®[1] nuclear power plant containment structure to a much higher internal pressure that could be encountered during a severe accident. In this study, for the prestressed containment structure, a detailed model is obtained by a full 3D model. Nonlinear finite element method is employed to predict the response of the structure using ANSYS software. The major challenges for modelling prestressing tendon elements are to accommodate parameters affecting prestressing forces. In previous research studies, the prestressing system is modelled using an equivalent pressure and tendon end forces, and tendons are modelled as smeared reinforcement in the concrete elements. In this study, the prestressing tendons are modelled using discrete elements. This method enables the capability of the model to update the prestressing forces accommodating the non-uniform losses. The difference in the response of the structure using the discrete model for the prestressing tendons and the smeared approach is 15 percent. It is observed that the containment structure, meets the design requirements of the current standards as it behaves linearly up to 1.5 times the design pressure, and the ultimate pressure capacity is estimated as 2.7 times the design pressure. The ultimate pressure capacity is reached when the prestressing tendon rupture at the dome.

Keywords: CANDU nuclear power plant, containment structure, finite element analysis, prestressed structure

1. INTRODUCTION

The containment system forms a continuous, pressure retaining envelope around the reactor core and the heat transport system. The containment structure (CS) protects the public and environment from all potential internal events, and is designed to withstand tornadoes, hurricanes, earthquakes and aircraft crashes; and to prevent the release of radioactive material to the environment. The containment structure contains of a cylindrical prestressed wall and a shallow dome. The perimeter wall (PW) is prestressed with a set of horizontal tendons and a set of vertical tendons. The shallow dome is prestressed with three sets of prestressing tendons. The entire structure is supported by a thick reinforced concrete base slab that ensures a fully enclosed boundary for environmental protection.

[1] CANDU® is a registered trademark of Atomic Energy of Canada Limited (AECL), used under exclusive license by Candu Energy Inc.

There is a demand in the nuclear power industry to investigate the response of containment structures to a much higher internal pressure that could be encountered during a severe accident. One of the design requirements for the nuclear power plant (NPP) containment structures is to have the ultimate pressure capacity (UPC) of at least twice the design pressure, and the structure to behave elastically to 1.5 times the design pressure. (CSA N287.3 2014)

The Finite Element Method (FEM) for structural analysis has been widely used in nuclear power industry. ANSYS is recommended as one of the most popular in both academic and commercial applications which is used in the current research study. (ANSYS Inc. 2010)

In abnormal conditions, such as Loss of Coolant Accident (LOCA), the containment structure is subjected to increasing internal pressure. Due to its low tensile capacity, concrete cracks easily when it undergoes tension. By increasing the internal pressure, the cracks penetrate through the thickness of the wall in the most weaken area. Then, the response is followed by the yielding of the reinforcing steel and high strength prestressing tendons.

The objectives of this study include introducing an appropriate model for concrete material that is capable of presenting the mechanical behavior of concrete under compression and tension as well as the behavior of concrete material after cracking. In addition to a proper model for the reinforcing steel that should incorporate a stress-strain curve that includes the initial linear response, yielding and post yielding response of the material. For pre-stressing tendon system, mechanical behavior under tension should be captured in the finite element model.

In previous research studies, the prestressing tendons are modelled as smeared reinforcement or shell layers in which the effects of prestressing system are applied as equivalent external pressures on the CS and as tendon end forces. It should be noted that in those studies, the non-uniform prestressing losses cannot be introduced to the model and were ignored.

The major challenges for modelling prestressing system are to accommodate parameters affecting prestressing forces. This includes: the geometry dependent changes along the tendon profile, changes due to incremental pressure and changes with time. In the current study, to introduce these critical changes, the discrete elements are used to model prestressing tendons. For discrete tendon elements, initial prestressing forces are addressed by an equivalent strain on each element. These elements are attached to concrete elements at coinciding nodes to transfer prestressing force to CS.

Using the discrete elements, the tendon layout is modelled as close as possible to the designed layout and enables the model to capture the most accurate results of the prestressing system. This approach significantly increases the complexity of the modelling; however, represents the most realistic modeling of the unsymmetrical tendon layout of the dome as well as of the perimeter wall.

The results of the two approaches are compared in this research study. In the current article, detailed pressure analysis is presented for a model prepared with discrete tendon elements in which the effects of the prestressing losses are included.

2. CONTAINMENT STRUCTURE PROPERTIES

2.1 Containment Geometry

The containment structure consists of a cylindrical perimeter wall, four buttresses at 90˚ intervals, a tori-spherical dome, a ring beam, a base slab and a tendon gallery. The meridional section of the containment is shown in Figure 1. The thickness of the perimeter wall in Candu containment structures is in range of 1000 mm to 1800 mm, and thickness of the dome is in rage of 600 mm to 1200 mm. The containment structure also contains of a steel liner at inner face of the PW and the dome to provide additional leakage protection.

The perimeter wall is prestressed with post-tensioning tendons. Tendons are anchored between alternate buttresses meaning that each tendon has an overlapping angular length just above 90˚ with another tendon. All the tendons are tensioned from both ends. This layout of horizontal tendons would create a close to uniform averaged tendon stress distribution. The perimeter wall is prestressed in meridional direction with vertical post-tensioning tendons. These

tendons are anchored at the bottom of the base slab in the tendon gallery and on top of the ring beam. All the vertical tendons are tensioned only from one end from the top of the ring beam.

The dome is prestressed with three layers of post-tensioning tendons. These tendons are placed in three layers which are at a 120˚ orientation with respect to each other. All the tendons in one layer have the same center and radius of curvature. All the tendons are tensioned from both ends and anchored at the vertical exterior side of the ring beam. The ring beam is prestressed in hoop direction with horizontal tendons. All the tendons have angular length of just above 180˚ and are tensioned from both ends.
The first step in the finite element modelling is to produce a proper geometry model of the structure. For the containment structure, the most detailed model is obtained by a full 3D model because of the unsymmetrical layout of the prestressing tendons at the dome.

It should be noted that the amount of hoop and meridional non-prestressing steels varies along the height of the perimeter wall, dividing the wall into 3 sections. Moreover, the amount of hoop and meridional non-prestressing steels for the dome varies along the height of the dome, dividing the dome to 2 sections.

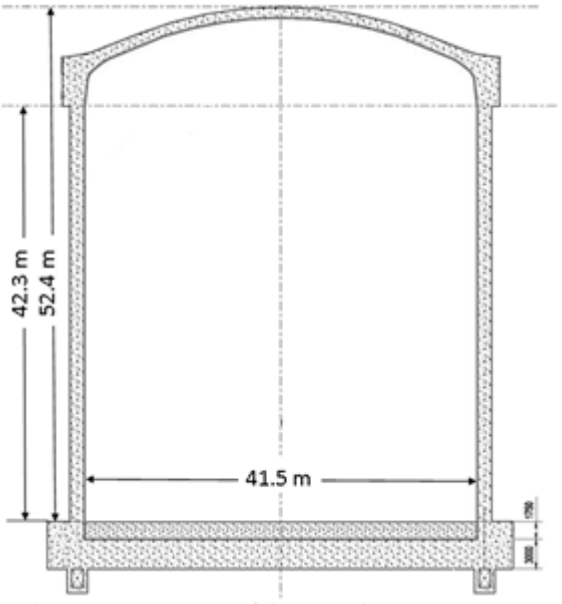

Figure 1: Geometry of the containment structure

2.2 Material properties

The structural materials used in the containment model in this paper are divided into three groups; which are concrete, non-prestressing steel and prestressing tendon.

For the concrete material in this study, the compressive and tensile strength are taken as 50 MPa and 5 MPa, respectively. For the elastic portion of the stress strain curve modulus of elasticity is 32,000 MPa and Poisson's ratio is 0.15.

For the prestressing tendon modulus of elasticity is 195,000 MPa. The ultimate tensile strength and yield strength are 1860 MPa and 1670 MPa, respectively. For non-prestressing steel, modulus of elasticity is 200,000 MPa and yield strength is 400 MPa. The bond between the reinforcements and concrete is assumed to be perfect.

3. FINITE ELEMENT MODEL

3.1 Element types

The CONCR model in ANSYS program enables the appropriate material model to account for both cracking and crushing parameters for concrete. Initially, concrete is treated as an incrementally linear elastic material. The isotropic properties for the material are defined as the modulus of elasticity and the Poisson's ratio.

For the concrete material model, the tri-axial failure surface model developed by (Willam and Warnke 1975) is employed. If the failure criterion defined for the material is not satisfied, there is no crack or crushing in the concrete. Otherwise, material crushes if the stress is compression. If the concrete material crushes at an integration point, it is assumed that there is no contribution to stiffness of the element at that point.

If the failure criterion is reached and the stress is in tension, material cracks. In the model, the cracking is determined by the criterion of maximum tensile stress, called "tension cutoff". Additional information that are needed for introducing the failure model are; shear transfer coefficients for an open crack and closed crack. It should be noted that, shear strength reverses due to aggregate interlocking and should be accounted for by introducing retaining positive shear strength. The typical values for the shear transfer coefficients are 0 to 1.0, with value of 0 representing a smooth crack with complete loss of shear transfer and value of 1.0 representing a rough crack with no loss of shear transfer. In this study, these values are assumed to be 0.35 and 0.6 for open cracks and closed cracks, respectively.

If the failure criterion is reached for all the planes in a tensile-tensile-tensile state, cracks are developed in the planes perpendicular to $\sigma1$ and $\sigma2$ and $\sigma3$. In the tension-tension-compression state, if the failure criterion reaches for $\sigma1$ and $\sigma2$, cracking occurs in the planes perpendicular to those perpendicular directions. Where $\sigma1$ and $\sigma3$ are the maximum and minimum of the three principal stresses in three principal directions, respectively. ($\sigma1 \geq \sigma2 \geq \sigma3$)

In the current study, 3D reinforced concrete elements, Solid-65, are employed. It should be noted that in the ANSYS program, only the Solid65 elements support the concrete material model. The isotropic Solid-65 is an 8-Node brick element that has three degrees of freedom (DOF) at each node, translation in X, Y and Z directions. This element is advantageous compared to the shell element employed in previous research studies, and is capable of introducing the contribution of the radial reinforcement. Moreover, the 3D solid elements are capable of modelling the nonlinear behaviour through thickness of the wall compare to conventional shell elements.

Two techniques are introduced in the program to model reinforcement. First is the smeared reinforcement approach, which assumes uniform distribution of reinforcing steel throughout the defined concrete elements. For the smeared reinforcement in solid65 element, the uni-axial stiffness of the reinforcement is added to the concrete element.

The smeared reinforcements are introduced by Real Constant (RC) Sets to the 3D reinforced concrete elements. Materiel number, volume ratio and orientation angel are the variables of the RC Sets. Each layer of reinforcing bars are assumed to be fully attached to the concrete elements, providing displacement compatibility between bars and concrete. As a result, the DOFs of the nodes at the rebar layers can easily be expressed in terms of the DOFs of the nodes at the external layers through the tri-linear shape functions in the concrete elements.

Second approach to model reinforcement is the discrete model, where bar elements are used to model the non-prestressing steel bars or prestressing tendons. Stiffness of the reinforcing bars is evaluated separately from that of the concrete elements. These elements are produced with displacement compatibility between bars and concrete. In this model, bar elements (Link8) are attached to concrete elements at coinciding nodes. The drawback of this model is that the concrete mesh is restricted by the location of the reinforcements.

The Link8 spar element is a uni-axial tension-compression element. This element has three degrees of freedom at each node; translation in X, Y and Z directions. For this approach, in the original finite element mesh, nodes should be located where the tendons are located. These coinciding nodes allow direct coupling between the concrete and tendon elements. To model the plastic behavior and large displacement for both non-prestressing steel bars and prestressing tendons, kinematic hardening model with von-Mises failure criterion is added.

3.2 Meshing details

Because some prestressing tendons and some non-prestressing steel bars are not placed axisymmetrically, the deformation of the containment is no longer axisymmetric, also this containment has no plane of symmetry. As a result, to capture more accurate results, the whole 3D containment structure is modelled in the finite element program.

In the finite element model, the height of the PW is divided into three sections along the height of the wall as shown in Figure 2. The reinforcing detail varies at inside face and outside face of the PW. Accordingly, PW is divided into 3 volumes through the thickness of the wall. Wall is divided to 6 elements through the thickness and to 142 elements along the height. The hoop and meridional non-prestressing steels are introduced as smeared reinforcements to the first two layers of concrete elements at inner face and two layers of concrete elements at outer face of the wall. The radial reinforcing steel are added as smeared reinforcements to all the elements for the PW.

Dome is divided into 74 elements along the arc of the dome and six layers in thickness. Meridional, hoop and shear non-prestressing steels are modelled as smeared reinforcements for the dome. The smeared meridional and hoop reinforcements are added to the first two layers of elements at inner face of the dome and the two elements at outer face of the dome. The shear reinforcing steel are added as smeared reinforcements to all the elements for the dome.

The prestressing tendons in the model are represented by Link8 elements. The effect of prestressing is added as an initial strain on the elements. The initial strain for each of the prestressing tendons can be calculated according the jacking force and properties of the tendon.

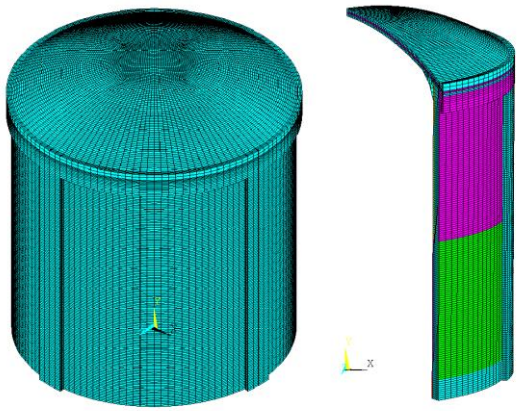

Figure 2: Reinforced concrete elements and real-constant sets

For the perimeter wall, 124 lines corresponding to the perimeter wall meridional cables are added with distance of 750 mm to interior surface and spacing of 1088 mm. Also, horizontal tendons are modelled with distance of 750 mm to interior surface of the perimeter wall. The finite element model also includes four buttresses at 90˚ intervals at which the horizontal tendons are anchored. Bar elements for wall horizontal tendons are connected at both ends to alternate buttresses meaning that each tendon has an angular length just above 180˚. Vertical spacing of the horizontal tendons in the FEM is 607 mm.

For the dome, tendons are placed in three layers which are at a 120˚ orientation with respect to each other. All the tendons in one layer have the same center and radius of curvature. All the lines representing the tendons are fixed from both ends to the vertical exterior side of the ring beam. Distance of the middle layer of the tendons in dome to interior surface if the containment is 550 mm.

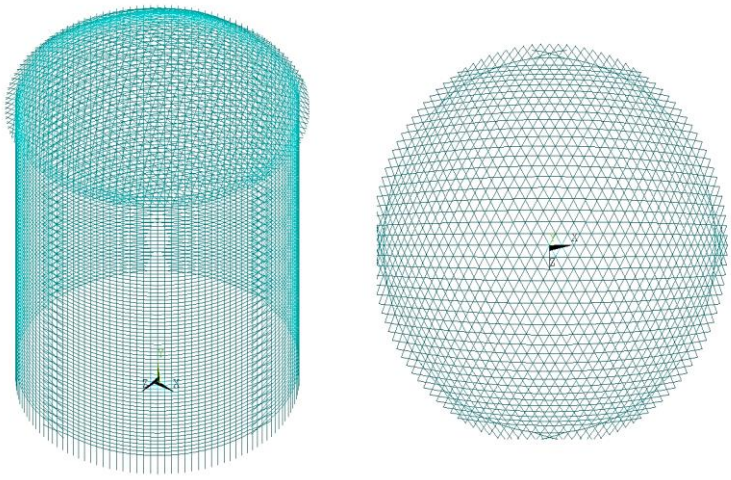

(a) (b)

Figure 3: Finite element of prestressing tendons for Model2 (a) 3D view, (b) Top view

Figure 3(a) and (b) show the elements for prestressing tendons using the Link8 elements for the perimeter wall, for the dome and for the ring beam. Figure 3(a) and (b) are the 3D view and top view of the model, respectively. To model the bond between the prestressing tendons and concrete; either, the coinciding concrete and tendon nodes are coupled together, or the displacement of the tendon nodes is calculated as the average of the two or three concrete nodes that are the closest to that tendon node. It should be noted that the tendon nodes that are coupled to concrete nodes, are assumed to have a 100% displacement compatibility. This assumption is appropriate for grouted tendons. This model is referred to as "Discrete Model" in this article.

In this article the effects of liner and base slabs are ignored and the model is fixed to the ground at the base. It should be noted that to prevent any premature failure due to stress concentration at locations of anchorage, a thick steel plate is added to the finite element model to simulate the anchorage system. 2D solid45 elements are used to model the plate.

Another model is also developed in which the prestressing tendons are added as smeared reinforcements. This model is referred to as "Smeared model" in this article. The reinforced concrete elements and meshes are prepared similar to that of Discrete Model. The material models, elements types, dimensions and assumptions are identical in these two models. It should be noted that the modelling effort for Discrete Model is much higher than that of the Smeared Model. Smeared Model has been previously used by several researcher as was mentioned before.

For the dome in the Smeared model, prestressing tendons are converted into equivalent meridional and circumferential reinforcements and added to the layer of concrete elements located at mid-depth of the dome (layers 3 and 4). For the perimeter wall, vertical reinforcements corresponding to meridional cables are added to the central layer of concrete elements; circumferential steel for the hoop prestressing is added to the central layer of elements. Also, hoop steel is provided in the ring beam to take into account the circumferential prestressing of this region. The effects of prestressing is added as an external pressure acting at outer face of the CS on the wall, dome and ring beam; in addition to tendon end forces for the wall vertical cables and dome horizontal cables.

The response of these two models are compared in this article in the form of internal pressure against normal displacement at dome apex to shown the effectivity of the Discrete Model. Detailed ultimate analysis for the CS under internal pressure and the effects of prestressing losses are only presented for the Discrete Model.

4. LOSSES OF PRESTRESSING FORCES

The prestressing losses in tendons are categorized to short-term and long-term losses. The short-term losses include elastic shortening of the concrete, anchorage set loss and friction loss in tendons. Prestressing force losses due to friction and anchorage set are geometry dependent. The long-term losses are time dependent, also dependent on the material behaviour such as creep and shrinkage of the concrete and relaxation of the prestressing tendons.

4.1 Geometry dependant losses

4.1.1 Friction loss

When a tendon is tensioned by a jack, the force produced is not constant along the length of the tendon due to friction between the tendon and the duct. The change in prestressing forces is caused because of the curvature frictional loss and the wobble frictional loss. During stressing, the force at location *x* along the tendon (*Px*) is given by equation (**Error! Reference source not found.**):

[1] $P_x = P_A e^{-\Sigma(\mu\alpha + Kx)}$

In equation (**Error! Reference source not found.**), μ and *K* are frictional coefficients, α is the intended angle change. In this study, P_A **is taken as the prestressing force at anchor.** (Collins and Mitchel 1991)

4.1.2 Anchorage set loss

The posttensioning system will result in additional loss in prestressing forces due to setting of the wedges. The length of the tendon affected by anchorage set is a function of the friction loss. If the friction is low, the length affected is larger. The anchorage set for the strand tendon (Δset) is 6 mm. The effected length is calculated according to equation (**Error! Reference source not found.**), where *p* is the average force loss due to friction per unit length. In equation (**Error! Reference source not found.**), A_{ps} and E_P represent area and modulus of elasticity of the tendon, respectively. (Collins and Mitchel 1991)

[2] $l_{set} = \sqrt{\frac{\Delta_{set} A_{ps} E_p}{p}}$

To introduce the variation of the prestressing forces along the length of the tendon, additional scripts are added to the program to change the forces of the elements according to the geometry and location of the elements. The variation of the strain along the circumferential length of a typical wall horizontal tendon is shown in Figure 4. The strain in the bar is directly proportional to the prestressing force of the tendon.

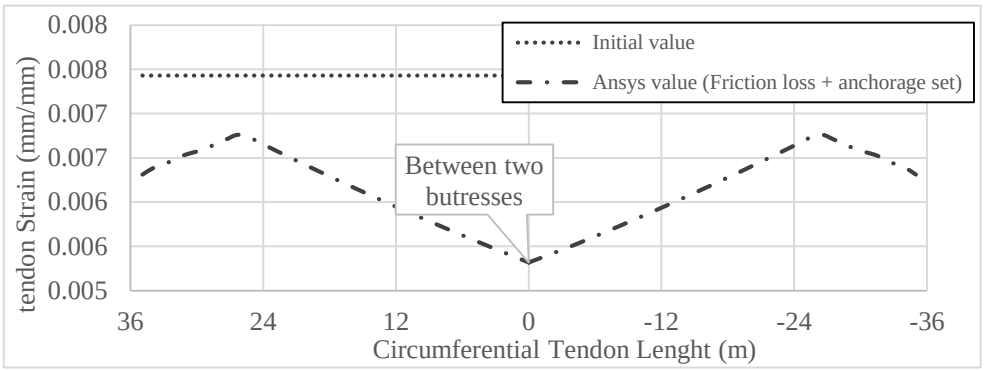

Figure 4: Variation of the strain in a typical PW circumferential tendon

4.2 Time dependant losses

4.2.1 Relaxation of tendon

Relaxation of the low relaxation tendons varies in an approximately linear function with the log of the time under stress. Relaxation of the steel can be accounted by using a reduced stiffness of the prestressing steel, $E_{p,eff}$. The reduced stiffness is calculated from equation (**Error! Reference source not found.**).

[3] $$E_{p,eff} = \left[1 - \frac{\log t}{45}\left(\frac{f_{pi}}{f_{py}} - 0.55\right)\right] E_p$$

Where t is the time under loads in hours, E_P is the initial modulus of elasticity, f_{pi} and f_{py} are the initial stress and the yield stress of the tendon.

4.2.2 Creep in concrete

The mechanical behaviour of the concrete in compression depends on the rate of loading and time history of loading. If the stress is held constant for some length of time, the strain increases. Same case goes to prestressed containment structure. If the containment structure is left under prestressing forces, creep due to material properties of concrete will result is changes in behaviour of the structure after several years. The effect of creep is accounted by reducing the initial stiffness of concrete (E_{ci}) on the stress strain curve. The creep coefficient at time t is calculated according to equation (**Error! Reference source not found.**):

[4] $$\emptyset(t, t_i) = 3.5\, k_c . k_f \left(1.58 - \frac{H}{120}\right) t_i^{-0.118} \frac{(t-t_i)^{0.6}}{10+(t-t_i)^{0.6}}$$

Where H is relative humidity in percent, k_c is a factor that accounts for the influence of the volume-to-surface ratio of the CS, and k_f is a factor accounting for the influence of concrete strength. Accordingly, the effective stiffness at time of t is $E_{c,eff} = \frac{E_{ci}}{1+\emptyset(t,t_i)}$. Comparison of the stress-strain curve for the prestressing tendons and concrete material at the time of prestressing and at the end of plant life is shown in Figure 5(a) and Figure 5(b), respectively.

4.2.3 Shrinkage in concrete

Shrinkage is a time-dependent moisture loss and as a result of this process, the volume of concrete is reduced. A simplified approach is used to account for shrinkage of concrete in the FE model. In this study, shrinkage strain is calculated according to the shrinkage between the time of prestressing and at the end of plant life. An equivalent negative temperature is applied on the concrete volume which is calculated according to equation **Error! Reference source not found.**.

[5] $$\Delta T = \frac{-k_s k_h \left(\frac{t}{t+35}\right) 0.51\times10^{-3}}{\alpha}$$

Where α is the coefficient of thermal expansion and for concrete equals to 10×10^{-6} $(^{\circ}C)^{-1}$, k_S is the cross-sectional shape factor, and k_h is the correction term for effect of humidity. (ACI209 2008)

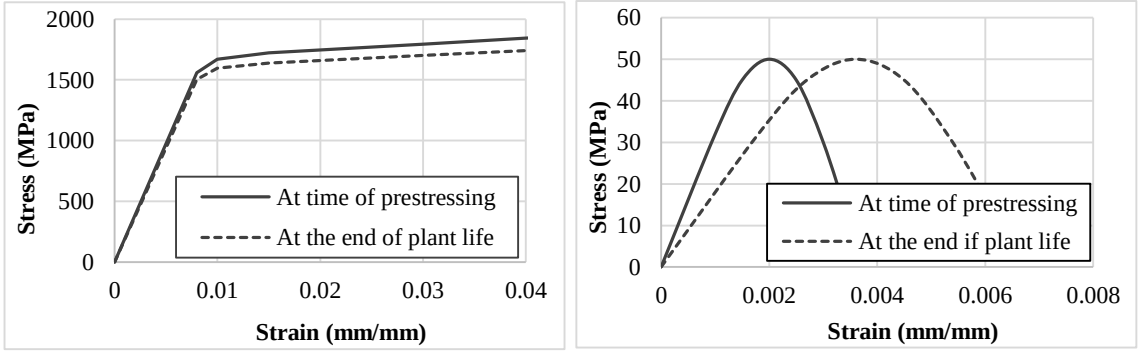

(a) (b)

Figure 5: Material properties at time of prestressing and at the end of plant life: (a) Prestressing tendon, (b) Concrete

5. LOADING CONDITIONS

The UPC analysis of the containment structure is conducted considering; dead loads, prestressing forces, and internal pressure. Although many possible accident scenarios exist and are important especially near the design pressure, in this study, for the calculation of ultimate pressure capacity of the containment, the effects thermal loads are ignored. The transient nature of the internal pressure is ignored as its period is much longer than that of the structure.

A static nonlinear finite element analysis is conducted to estimate ultimate pressure capacity of the CS. Because of small displacement in concrete containments, geometry non-linearity or thinning of the wall need not to be accommodated in the model. It should be noted that the full Newton-Raphson method of analysis is used to compute the nonlinear response. The Newton-Raphson method is an iterative process of solving the nonlinear equations. This method updates the stiffness matrix at each iteration. As a result, the load is applied incrementally to the structure up to the failure.

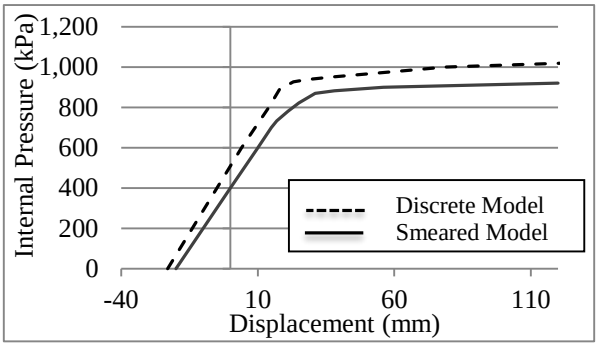

Figure 6: Comparison of Smeared Model and Discrete Model

6. RESULTS AND DISCUSSION

6.1 Comparison of Smeared model and Discrete Model

The response of the structure in the form of the internal pressure against the normal displacement at dome apex is compared for the two approaches in Figure 6. Both the models are analysed ignoring all the geometry dependant and the time dependent prestressing force losses. To reduce computational effort analysis are stopped when the dome starts to go under excessive deformation. More detailed comparison of the response of these two models are presented in another article by the authors. (Tavakkoli et al. 2015)

It is observed that in both models, the CS behaves linearly up to 1.5 times the design pressure. However, for the Discrete Model, the linear limit is higher in comparison to the Smeared model. The value of the pressure capacity is increased by 15% in comparison with the Smeared model.

It is concluded that the Discrete Model represent a more realistic model of the prestressing system and is able of introducing the non-uniform prestress losses. Discrete model enables the finite element model to capture the complicated layout of prestressing tendons for the dome and the PW. Using Discrete Model, the geometry dependent prestressing losses and changes in the prestressing forces can explicitly introduced to the model. It should be noted that, modeling effort for the Discrete model is more intensive in comparison with the Smeared model. For pressure analysis within the linear limit of the CS, both models give satisfactory results.

6.2 Overall behaviour of the containment structure under increasing internal pressure

The response of the containment structure introducing all prestressing losses are shown in Figure 7(a) and Figure 7(b), in the form of the internal pressure against normal displacement at dome apex and mid-height of the PW, respectively. Should be noted that the positive normal displacement at dome apex is upward deformation and positive normal displacement at wall mid-height is an outward deformation.

For this model, the first crack develops at internal pressure of 708 kPa at the dome, due to radial stress. Radial reinforcement yields at dome apex at internal pressure of 708 kPa. At internal pressure of 738 kPa, cracks form at dome lower elevation due to both hoop and radial stresses. Next critical steps are internal pressure of 818 kPa at which the prestressing tendon yields at lower elevation of the dome and at internal pressure of 869 kPa at dome apex.

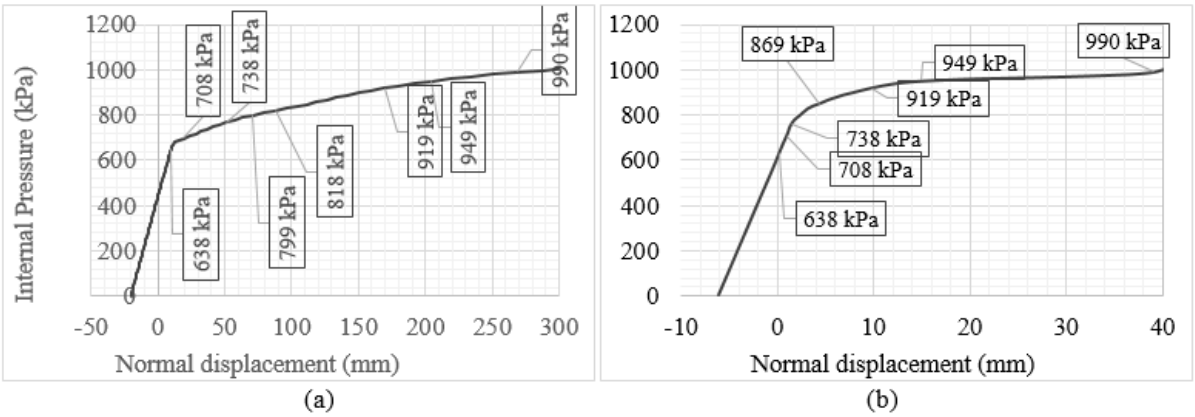

Figure 7: Internal pressure vs. normal displacement: (a) at dome apex, (b) at PW mid-height

At internal pressure of 919 kPa, vertical cracks develop at PW progressing along the height of the wall. At pressure of 990 kPa, vertical tendon yields at the PW and is followed by the failure of the FEM at internal pressure of 1070 kPa when the prestressing tendon ruptures at the dome.

According to US Nuclear Regulatory Commission recommendation, the pressure capacity may be estimated based on satisfying both of the following strain limits: (CSA N287.3 2014)

1. Total tensile average strain in tendons away from discontinuities of 0.8 percent
2. Global free-field strain for reinforcing steel, concrete and liner of 0.4 percent.

For the CS, the tendon first yields at internal pressure of 798 kPa and the maximum tensile strain of 0.4 percent is reached at internal pressure of 900 kPa. Accordingly, the functional integrity limit for the containment structure is 798 kPa and the structural integrity limit for the containment structure is 1070 kPa.

7. CONCLUSIONS

The objective of this article is to investigate the response of a CANDU containment structure to a much higher internal pressure that could be encountered during a severe accident. The major challenges for modelling the prestressing system are to accommodate parameters affecting prestressing forces. In previous studies, the prestressing system is modelled using an equivalent pressure in addition to tendon end forces to represent the prestressing forces, and the prestressing tendons are modelled as smeared reinforcements. This approach presents no difficulty modelling the prestressing system; however, any non-uniform change in the prestressing forces cannot be directly accommodated. In this study, an alternative approach is employed to capture the prestressing system, in which the prestressing tendons are modelled using discrete elements and prestressing forces are applied directly to tendon elements as initial strain. This method is more appropriate when the tendons are not located in an axisymmetricall or a symmetrical fashion. Moreover, the proposed approach has the capability to update the prestressing forces accommodating the non-uniform losses in prestressing forces.

In this study, it is observed that the pressure capacity of the containment structure is dependent on how the prestressing system is modelled. When the prestressing tendons are modelled as smeared reinforcement (Smeared Model) and the effects of prestressing system are added as an equivalent pressure and forces on the CS, the pressure capacity is reduced by 15%, in comparison with the Discrete Model. Although the later approach increases the complexity of the modelling, but is a more appropriate way to model the prestressing system of the CS in which tendon layout is not symmetrical. To predict the linear limit of the structure, both method showed satisfactory results and the pressurized CS remains linear beyond 1.5 times the design pressure.

Detailed ultimate pressure analysis is conducted on the Discrete Model. Moreover, all the geometry and time dependent prestressing force losses are included in the model. It is observed that for this containment structure, the first crack forms at dome of the structure close to the ring beam at 1.8 times the design pressure. The crack forms due to excess of radial stress. With increase of internal pressure, more cracks form due to radial stress closer to apex of the dome. The elements continue to crack in radial direction when the stiffness is reduced due to the first crack. The response is then followed by yielding of the hoop reinforcement at dome followed by yielding of radial reinforcement.

The first tendon yields at the dome closer to the ring beam at internal pressure more than two times the design pressure. With increase of internal pressure the number of yielded tendons increases in the same vicinity. At the end of the analysis, concrete elements are cracked in all directions. Due to excessive deformation, the analysis stops finally at internal pressure of 1070 kPa. This occurs when the prestressing tendon ruptures at the dome. The ultimate pressure capacity of this containment structure is estimated as 2.7 times the design pressure.

ACKNOWLEDGEMENTS

This project was initiated as a joint effort between Ryerson University, SNC-Lavalin and Candu Energy Inc. Authors would like to thank SNC-Lavalin Inc., Candu Energy Inc., Mitacs Accelerate PhD program and Ryerson University for their financial support throughout this research study.

REFERENCES

ACI Committee 209, (2008). Guide for Modeling and Calculating Shrinkage and Creep in Hardened Concrete, ACI209.2R-08, American Concrete institute, Detroit

ANSYS Inc. (2004). ANSYS help manual (Version 11.1), Global headquarters, Southpointe, 275 Technology drive, Canonsburg, PA.

ANSYS software (Version 12.1). (2010). Global headquarters, Canonsburg, Pennsylvania.

Collins, M. P., and Mitchell, D. (1991). Prestressed concrete structures (Vol. 9). Englewood Cliffs, NJ: Prentice Hall.

CSA N287.3-14 (2014): Design Requirements for Concrete Containment Structures for CANDU Nuclear Power Plants: Revision (2009), Canadian Standard Association, Toronto, ON.

Tavakkoli, I., Kianoush M.R., Abrishami H, Han X.M. (2015), Nonlinear finite element analysis to predict ultimate pressure capacity of a nuclear power plant containment structure, " In Proceedings, 2015 CSCE Annual Conference, Regina, Canada.

Willam, K. J., and Warnke, E. P. (1975). Constitutive model for the tri-axial behavior of concrete. In Proceedings, International Association for Bridge and Structural Engineering (Vol. 19, p. 174). ISMES, Bergamo, Italy.